Fabrication of size-selected Pd nanoclusters using a magnetron plasma sputtering source

A. I. Ayesh,[a] N. Qamhieh, H. Ghamlouche, S. Thaker, and M. El-Shaer
Department of Physics, United Arab Emirates University, Al Ain, P.O. Box 17551, United Arab Emirates

(Received 21 October 2009; accepted 22 December 2009; published online 11 February 2010)

We report on the fabrication of palladium (Pd) nanoclusters using a dc magnetron sputtering source. Plasma sputtering vaporizes the target's material forming nanoclusters by inert gas condensation. The sputtering source produces ionized nanoclusters that enable the study of the nanoclusters' size distribution using a quadrupole mass filter. In this work, the dependence of Pd nanoclusters' size distribution on various source parameters, such as the sputtering discharge power, inert gas flow rate, and aggregation length have been investigated. This work demonstrates the ability of tuning the palladium nanoclusters' size by proper optimization of the source operation conditions. The experimental nanocluster sizes are compared with a theoretical model that reveals the growth of large nanoclusters from "embryos" by a two-body collision. The model is valid for a specific range of deposition parameters (low inert gas flow rates and aggregation lengths equal or below 70 mm).
 [doi:10.1063/1.3296131]

I. INTRODUCTION

Formation of nanoclusters has generated great deal of interest because of their properties which are not found in corresponding macroscopic systems. A main objective of researchers in this field is to study the variation in nanoclusters' properties as their sizes increase in order to understand the evolution of the physical and chemical properties with the growth from atoms to bulk. This requires controlled fabrication of nanoclusters with tailored size. Hence, rigorous research effort is needed to address different size control parameters, such as collision dynamics, nucleation dynamics, and equilibrium and nonequilibrium properties of fluid-solid interfaces.[1]

dc plasma sputtering provides a simple method for nanoclusters' production and can be used for large range of nanocluster materials.[2] An electric field between the plasma and the biased target accelerates argon (Ar) ions which cause the sputtering of atoms and small nanoclusters from the target. Next, nanocluster aggregation occurs in an inert gas atmosphere. Nanocluster production using sputtering sources become a popular technique because of many advantages. For example, about 30% of the produced nanoclusters are ionized;[3] therefore nanocluster size selection technique can be applied without any further ionization stage. Moreover, the influence of deposition energy on the nanocluster morphology (when deposited on a substrate) can be controlled by adjusting the source parameters. In addition, the produced nanoclusters using a sputtering source are without passivation layers which provide direct access to their surface properties.

The study of the growth parameters of palladium (Pd) nanoclusters is important because of their diversity of applications such as catalysts[4] and hydrogen sensor.[5] In this context, various source parameters that determine the nanocluster size distribution such as the dc sputtering discharge power, inert gas flow rate, and aggregation length are investigated in details. To the best of our knowledge, there are very few reports[4,6,7] that discussed the effect of different source parameters on the size distribution of Pd nanoclusters. In addition, this is the only study that compares experimental size results of Pd nanoclusters to a theoretical model of nanocluster growth by a two-body collision process.

II. NANOCLUSTER SIZE MODEL

Theoretically, nanocluster growth into large nanocluster can be explained in terms of two-body collision. Knauer[8] used the homogenous nucleation theory to introduce a model that describes the nanocluster growth by the add-atom process. The model was used to explain the growth of nickel, copper, and silicon nanoclusters produced using magnetron sputtering sources.[9,10] The nanocluster growth rate can be expressed as[8]

$$\frac{di}{dt} = v_z \frac{di}{dz} = \pi (r_a + r_c)^2 n v_{\text{th}} \beta, \tag{1}$$

where i is the number of atoms per nanocluster, v_z is the vapor velocity, r_a and r_c are the radii of atom and nanocluster (respectively), n is the vapor density, z is the nanocluster traveling length, v_{th} is the mean velocity with the reduced mass of the i-sized nanocluster, and β is the nanocluster growth-retarding effect due to the high latent heat of condensation of metals. Equation (1) can be solved using Mach number (M)

$$M = v_z \left(\frac{\gamma k_B T}{m_a} \right)^{1/2} \tag{2}$$

and the approximation,

[a]Electronic mail: ayesh@uaeu.ac.ae.

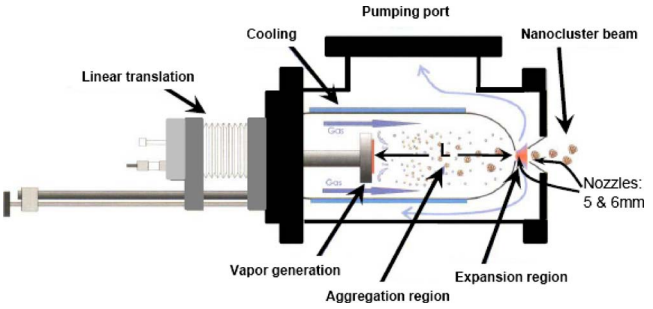

FIG. 1. (Color online) Schematic diagram of the cluster source, after Ref. 11.

$$r_a + r_c \cong r_c = \left(\frac{3}{4\pi}\right)^{1/3} i^{1/3} a_v, \tag{3}$$

where $r_c \gg r_a$, m_a is the mass of the vaporized atom, and a_v is the interatomic distance ($=2r_a$). Therefore, solving Eq. (1) gives

$$i^{1/3} = i_o^{1/3} + \left(\frac{4\pi}{3}\right)^{1/3} \left(\frac{1}{2\pi\gamma}\right)^{1/2} a_v^2 \int_{z=0}^{\infty} \frac{\beta n}{M} dz, \tag{4}$$

where i_o is the size of a critical embryo.

III. EXPERIMENTAL

Pd nanoclusters were synthesized using a magnetron sputtering plasma aggregation source inside a commercial ultrahigh vacuum compatible system (Nanogen-50, Mantis Deposition Ltd., Oxfordshire, U.K.). Two turbo pumps were used to evacuate the main and source chambers to a base pressure of $\sim 10^{-8}$ mbar. The dc magnetron type discharge was used to generate clusters from a 99.95% purity Pd target with a discharge power up to 40 W. Argon gas with 99.999% purity has been used to generate the plasma and to aggregate Pd nanoclusters from the target which is fixed on magnetron sputter head. A MKS Instruments mass flow controller was used to control the Ar flow rate (f) in the range of 10–100 SCCM (SCCM denotes standard cubic centimeter per minute). The magnetron gun and the source walls were water cooled.

The magnetron gun was mounted on a linear translator with a motor, enabling the aggregation length (L) (defined as the distance from the sputtering target surface to the source exit nozzle) to be varied up to 100 mm (see Fig. 1). The gas stream sweeps the nanoclusters outside the source into the main chamber through two nozzles (diameters of 5 and 6 mm in order) at the exit of the source chamber, where the nanocluster growth stops. A directed nanocluster beam is formed once the nanoclusters leave the 6 mm nozzle. The produced nanoclusters can be deposited on a substrate fixed on a sample holder which is mounted on a vertical motorized linear translator. The nanoclusters deposition rate is measured using a quartz crystal monitor (QCM). The QCM is fixed on a motorized linear translator that enables driving the QCM in front of the exit nozzle, check the deposition rate, and then drive it back away from the beam path. The position of the liner translators holding the magnetron gun, QCM, and sample holder can be varied without venting the system.

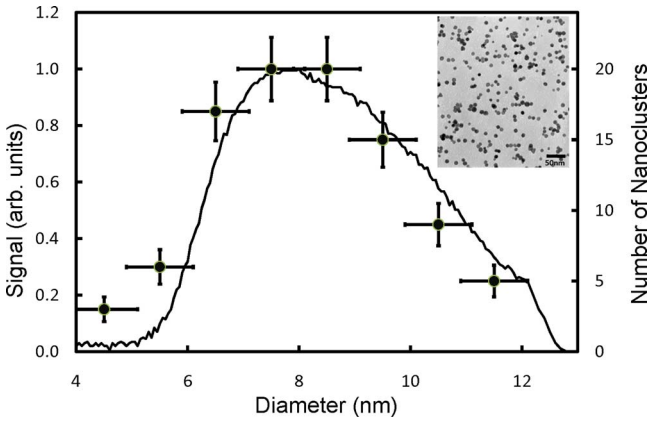

FIG. 2. (Color online) The solid line is the size distribution of Pd nanoclusters produced using the quadrupole mass filter. The circles are the results found from the TEM images. The inset is a high resolution TEM image of Pd nanoclusters produced using the same source conditions as those used for the size distribution in the figure.

A quadrupole mass filter consisting of four parallel metal rods was used to measure the nanocluster size distribution inside the source chamber. Each pair of opposite rods is connected together electrically to potentials of $[U+V\cos(\omega t)]$ and $-[U+V\cos(\omega t)]$, where U is a dc voltage and $V\cos(\omega t)$ is an ac voltage. In each size distribution scan, the ratio U/V was fixed and the mass distribution was scanned by varying the frequency, ω. The resolution of the filter is adjusted for a mass scan by setting the U/V ratio up to 0.168. A grid located at the exit of the mass filter has been used to measure the ion flux of the selected mass/size, and the resultant current is measured by a picoammeter. It should be noted that in our previous work,[6] the size distribution of nanoclusters has been studied using a parallel plate mass filter. The nanocluster size distribution was corrected by dividing the measured signal by mass (M) since the mass resolution ($\Delta M/M$) was fixed over the entire mass range; which means that the range of the mass being detected (ΔM) is proportional to M. However, in the current study the ratio U/V is activated as a function of the mass number such that the actual resolution $\Delta M/M$ does not remain constant but ΔM does.[12] Therefore, no need to apply any correction.

A Philips CM10 transmission electron microscope (TEM) has been used to confirm the size distribution measured by the quadrupole mass filter. Pd nanoclusters were deposited on carbon-coated copper microgrids at room temperature.

IV. RESULTS AND DISCUSSION

The solid line in Fig. 2 shows the size distribution of Pd nanoclusters measured using the quadrupole mass filter. The nanoclusters were produced using a discharge power of 18.9 W, $f=40$ SCCM, chamber pressure $P=7.9\times10^{-4}$ mbar, $U/V=0.12$, and $L=90$ mm. The figure shows that the peak diameter is about 7.7 nm. TEM images of Pd nanoclusters produced using the above source conditions and have not been mass selected (an example is shown in the inset of Fig. 2) were used to confirm the size distribution measured by the mass filter. The filled circles with error bars in Fig. 2 are the

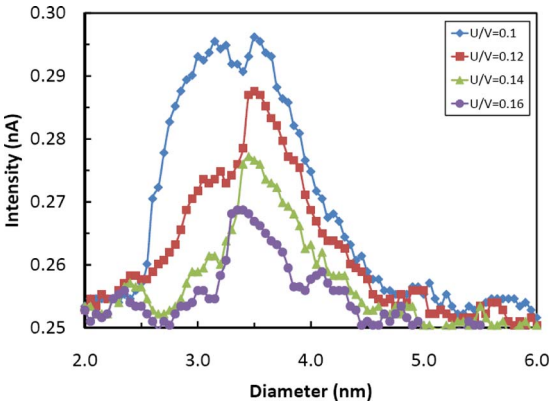

FIG. 3. (Color online) The effect of the U/V ratio on the nanocluster size distribution.

results taken from the TEM image. The TEM results are in good agreement with the size distribution produced by the mass filter.

Figure 3 shows the effect of changing U/V on the size distribution produced using a discharge power of 6.8 W, $f=20$ SCCM, $P=3.6\times10^{-4}$ mbar, and $L=50$ mm. The figure depicts that as U/V increases the nanocluster ion signal decreases, and it illustrates different features within the size distribution. However, the size distributions remain within the range of 2.2–4.6 nm as the U/V changes. Figure 3 also shows that a U/V of 0.12 produces a reasonably strong signal while maintaining the distribution features; therefore this value (0.12) was used for the rest of this work. It is worth noting that a bimodal distribution is observed in Fig. 3, but is not seen in the rest of the size distributions with different conditions (see for example Fig. 2). Therefore, the observed bimodal distributions are not universal for all produced nanocluster distributions. Other investigators[13–15] have observed bimodal distributions for nanoclusters deposited on substrates after annealing, and they[14] concluded that their bimodal distributions were not universal too.

The dc sputtering discharge power is a main factor affecting nanocluster production. An inadequate discharge power would not produce sufficient self bias on the target, thus, nanoclusters cannot be detected. The effect of the sputtering discharge power on the size distribution is shown in Fig. 4(a) for $f=20$ SCCM, $P=3.6\times10^{-4}$ mbar, and $L=50$ mm. The Pd nanoclusters could be detected only within a discharge power range of 6.8–37.6 W. The figure shows that the number of nanoclusters increases as the discharge power increases from 6.8–11.6 W. However, further increase in the discharge power decreases the number of nanoclusters. The figure also shows that increasing the discharge power from 6.8 to 24 W shifts the distribution peak toward larger nanoclusters. Further increase in the discharge power decreases the distribution peak to smaller nanoclusters as shown in Fig. 4(b). The term "peak diameter" is used to describe the nanocluster diameter at the maximum of the size distribution curve.

The magnetron-based source has an advantage in terms of the wide nanocluster size range. The variation in nanocluster size is dependent on several parameters, such as the aggregation length and inert gas flow rate. The dependence

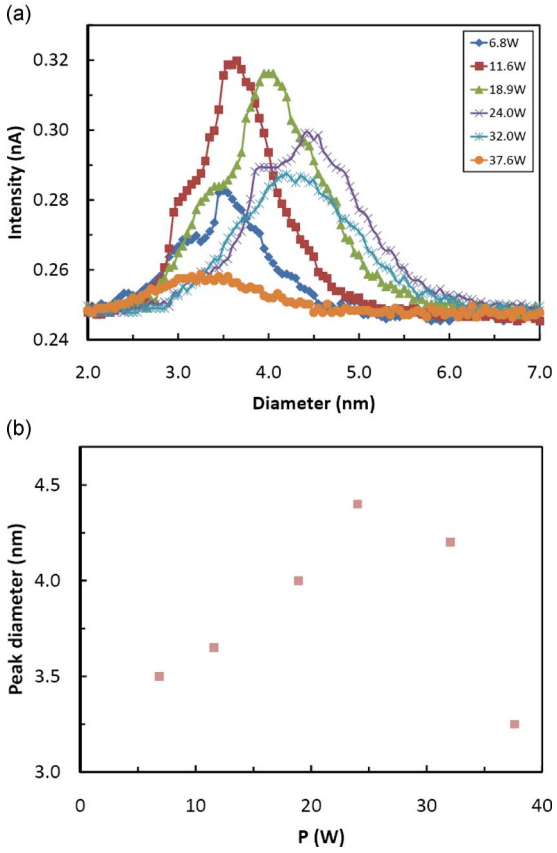

FIG. 4. (Color online) (a) The effect of the sputtering discharge power on the nanocluster size distribution. (b) The dependence of the peak diameter on the sputtering discharge power.

of the peak diameter on argon flow rate for aggregation lengths between 30 and 90 mm is shown in Fig. 5. The results are produced using a discharge power of 18.9 W and pressure in the range of 3.6×10^{-4}–2.1×10^{-3} mbar. The nanocluster peak diameters in Fig. 5 were taken from size distribution curves similar to those in Fig. 4(a). Figure 5 shows that for L between 40 and 70 mm the nanocluster size initially increases with f to a peak value and then decreases

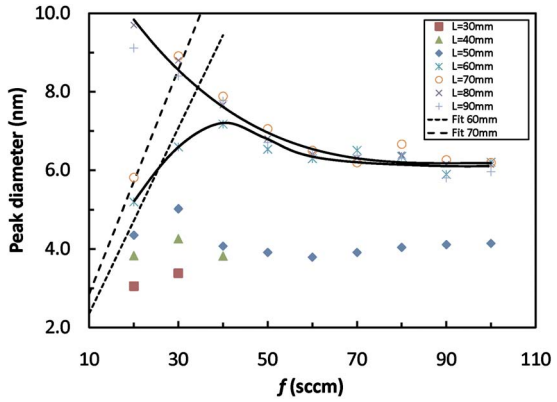

FIG. 5. (Color online) The dependence of the peak diameter on Ar flow rate for aggregations lengths in the range of 30–90 mm. The dashed lines are the theoretical nanocluster size calculation for $L=60$ and 70 mm. The solid lines serve as guide to the eye to show zones I (the increase in the peak diameter with f for $L=60$ mm and $f\leq40$ SCCM), and zone II (the decrease in the peak diameter with f for $L=80$ mm, or for $L=60$ mm and $f\geq40$ SCCM).

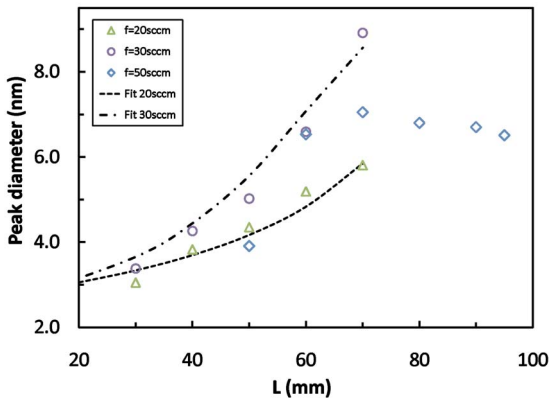

FIG. 6. (Color online) The dependence of the peak diameter on L for $f=20$, 30, and 50 SCCM. The dashed lines are the theoretical nanocluster size calculations for $f=20$ and 30 SCCM.

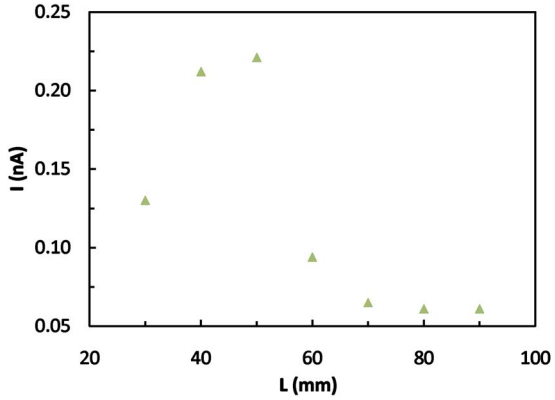

FIG. 7. (Color online) The dependence of the nanocluster current signal of the peak diameter on L for $f=30$ SCCM.

before it stabilizes and becomes almost constant. However, for $L=80$ and 90 mm the nanocluster diameter decreases with f (between 20 and 60 SCCM) and then it becomes constant. For $L=30$ mm there are only two measurable data points where the peak diameter increases with f.

The observed phenomenon is discussed in terms of nanocluster production which occurs initially through the nucleation of nanocluster seeds due to cooling of the sputtered atoms by Ar. The seed production is described as three-body collision: two sputtered atoms and one Ar atom to remove the excess kinetic energy from the sputtered atoms. The probability of the three body collision increases as the density of atomic vapor increases. Therefore, minimum sputtering discharge power and Ar flow rate are required to initiate the three body collision. Also the nanocluster peak diameter is expected to decrease as f increases because of the high drift velocity of the material within the growth region; hence, the collision probability decreases. The nanocluster seeds are then nucleate into large nanoclusters. This process, described as two-body collision, may occur through nanocluster growth via atomic condensation and nanocluster-nanocluster collision.[9,16] Consequently, larger nanoclusters are produced as f increases.

The variation in the nanocluster peak diameter as a function of f and L shown in Fig. 5 could be understood in terms of each mechanism contribution, i.e., nucleation of nanocluster seeds and nucleation of large nanoclusters. As the peak diameter increases with increasing f, the nucleation of large nanoclusters is the dominant mechanism (zone I), and it occurs for low f and L between 30 and 70 mm. However, when the nucleation of new seeds becomes dominant the nanocluster peak diameter decreases as f increases. This region is called zone II where the nucleation of new seeds is the dominant mechanism for $L=80$ and 90 mm. It also occurs for $f \geq 40$ SCCM and L between 40 and 70 mm. The dominance of the three-body collision at $L=80$ and 90 mm and low f (although the low atomic vapor density) can be attributed to the long nucleation time which causes further three-body collisions.[9,10]

To explore more the effect of the aggregation length on the nanoclusters size, Fig. 6 shows the variation in the peak diameter as a function of L for $f=20$, 30, and 50 SCCM (P of 3.6×10^{-4} and 1.0×10^{-3} mbar) and a discharge power of 18.9 W. In the figure, $f=20$ and 30 SCCM are taken as examples of zone I, while $f=50$ SCCM is taken for zone II. The figure shows a direct increase in the peak diameter with L for $f=20$ and 30 SCCM, while for $f=50$ SCCM the peak diameter increases initially from ~3.9 to ~6.8 nm and then remains almost constant. Similar dependence (to that of $f=50$ SCCM) can be observed for f greater than 50 SCCM.

The direct increase in the nanocluster peak diameter with L, observed in Fig. 6 for $f=20$ and 30 SCCM (zone I), can be understood in terms of the nucleation time. Increasing the aggregation length allows the nanocluster to remain longer within the aggregation region which causes the growth of the nanocluster size. For nanoclusters within zone II ($f=50$ SCCM), the initial increase in the nanocluster peak diameter with L (for $L\leq70$ mm) can be also understood in terms of the nucleation time. However, at $L>70$ mm the nanocluster density decreases with their growth and it takes longer time for three-body collisions[9] which compensate the effect of the nucleation time. Hence, the diameter remains almost constant.

In addition to the sputtering discharge power, L and f need to be optimized as well. For example, Pd nanoclusters were only produced with a significant signal for $L=30$ mm when $f\leq30$ SCCM (see Fig. 5). This is illustrated in Fig. 7 which shows the dependence of nanocluster signal of the peak diameter on L for $f=30$ SCCM, $P=5.7\times10^{-4}$ mbar, and a discharge power of 18.9 W. The figure reveals that the best current signal is between $L=30$ and 60 mm while beyond $L=60$ mm the nanocluster signal decreases significantly. It should be noted that nonmeasurable nanocluster signal does not necessarily mean that nanoclusters are not produced.

Since the nanoclusters size range is determined by different inter-related factors, the operation conditions need to be varied properly to obtain a wide size range. The process starts by injecting the source with a reasonable gas flow rate with a careful adjustment to the sputtering discharge power and aggregation length.

Pd nanocluster sizes have been evaluated using Eq. (4) within zone I as a function of f and L at constant β ($\beta=\beta_o$). In addition, n and M vary along the free jet according to the following approximations[8]

$$n \cong \frac{1}{4} n_o \left(\frac{L}{d}\right)^{-2} \tag{5}$$

and

$$M \cong 3\left(\frac{L}{d}\right)^{2/3}, \tag{6}$$

where d is the nozzle diameter and L corresponds to z in Eq. (4). n_0 can be replaced by p/k_BT, where p is the source pressure, k_B is Boltzmann constant, and T is the temperature in kelvin. The following parameters have been used to evaluate the nanocluster size: $i_o=7(r_a)$,[1] $r_a=1.37\times10^{-10}$ m, $\gamma=5/3$, $\beta_o=5\times10^{-2}$,[8] and $d=5$ mm.

The theoretical nanocluster sizes interpreted by the model are compared with the experimental data within zone I. The dashed lines in Fig. 5 are the calculated size for $L=60$ and 70 mm, while the dashed line in Fig. 6 is the calculated size as a function of L for $f=20$ and 30 SCCM. The theoretical size calculations fit well with the experimental results (within zone I) for $L=70$ mm in Fig. 5, and for $f=20$ and 30 SCCM in Fig. 6. The fit is also close to the data points at $f=20$ and 30 SCCM for $L=60$ mm in Fig. 5. This indicates that the nanocluster production for the above conditions is dominated by the two-body collision mechanism. This is consistent with our argument that, within zone I, nanoclusters nucleate into large nanoclusters from embryos. However, for the data point at $L=60$ mm and $f=40$ SCCM in Fig. 5, a possible contribution of three-body collision mechanism could be the reason of discrepancy between the fit and the experimental data. Therefore, this point cannot be considered within zone I. It should be noted that as f increases and L decreases the probability of three body collisions increases. It is also obvious that the data points within zone II in Figs. 5 and 6 have different trend to the model: in Fig. 5 the experimental size decreases with f instead of increasing as for the model (see for example the size for $L=80$ mm), and in Fig. 6 the experimental size for $f=50$ SCCM increases with L and then decreases. These observations indicate that within zone II the three-body collision is more favorable.

V. CONCLUSION

The growth of Pd nanoclusters in a sputtering gas aggregation source was investigated. The nanocluster size distribution was varied between 2 and 10 nm by tuning the source parameters, i.e., the sputtering discharge power, inert gas flow rate (f), and aggregation length (L). We found that the inert gas flow rate and aggregation length have the greatest effect on changing the nanocluster size. In general, the results showed that increasing the aggregation length leads to the production of large nanoclusters due to the increase in the nucleation time. The nanocluster peak diameter variation reveals two nucleation mechanisms occur within the aggregation region: nucleation of large nanoclusters where the nanocluster size increases as f increases, and nucleation of new nanocluster seeds which leads to a decrease in the nanocluster size with f.

The variation in Pd nanocluster size with f and L was compared with a theoretical model that describes the nanocluster growth in terms of two-body collision (for low f and $L\leq70$ mm). We have found that the experimentally obtained sizes are reasonably concurrent with the theoretically calculated values obtained from this model.

ACKNOWLEDGMENTS

This work was supported by the United Arab Emirates University under a Grant No. 03-02-2-11/09. The authors would like to thank Mr. S. Tariq at FMHS, United Arab Emirates University for the TEM imaging.

[1] M. Kappes and S. Leutwyler, in *Molecular Beams of Clusters in Atomic and Molecular Beam Methods*, edited by G. Scoles (Oxford, New York, 1988), Vol. 1.
[2] S. Yatsuya, T. Kamakura, K. Yamauchi, and K. Mihama, Jpn. J. Appl. Phys., Part 2 **25**, L42 (1986).
[3] H. Haberland, M. Karrais, M. Mall, and Y. Thurner, J. Vac. Sci. Technol. A **10**, 3266 (1992).
[4] R. Wsuurschum, K. Reimann, S. Gruss, S. A. Kubler, P. Scharwaechter, W. Frank, O. Kruse, H. D. Carstanjen, and H. E. Schaefer, Philos. Mag. B **76**, 407 (1997).
[5] J. van Lith, A. Lassesson, S. A. Brown, M. Schulze, J. G. Partridge, and A. Ayesh, Appl. Phys. Lett. **91**, 181910 (2007).
[6] A. I. Ayesh, A. Lassesson, S. A. Brown, A. D. Dunbar, M. Kaufmann, J. Partridge, R. Reichel, and J. van Lith, Rev. Sci. Instrum. **78**, 053906 (2007).
[7] R. Reichel, J. G. Partridge, A. D. F. Dunbar, S. A. Brown, O. Caughley, and A. Ayesh, J. Nanopart. Res. **8**, 405 (2006).
[8] W. Knauer, J. Appl. Phys. **62**, 841 (1987).
[9] T. Hihara and K. Sumiyama, J. Appl. Phys. **84**, 5270 (1998).
[10] A. N. Banerjee, R. Krishna, and B. Das, Appl. Phys. A: Mater. Sci. Process. **90**, 299 (2007).
[11] *Nanogen-50 User Manual* (Mantis Deposition Ltd., Oxfordshire, 2009).
[12] P. H. Dawson, *Quadrupole Mass Spectrometry and its Applications* (Elsevier, Amsterdam, 1976); *Pfeiffer Quadrupole Mass Filter User Manual* (Pfeiffer Vacuum GmbH, Germany, 2009).
[13] A. Thomann, J. Salvetat, Y. Breton, C. Andreazza-Vignolle, and P. Brault, Thin Solid Films **428**, 242 (2003).
[14] A. Howard, C. Mitchell, and R. Egdell, Surf. Sci. Lett. **515**, L504 (2002).
[15] B. Kumar and R. Soni, Nucl. Instrum. Methods Phys. Res. B **266**, 2576 (2008).
[16] J. M. Soler and N. Garcia, Phys. Rev. Lett. **49**, 1857 (1982).